https://doi.org/10.1016/j.msea.2021.141495

Severe plastic deformation-produced gradient nanostructured copper with a strengthening-softening transition

Bo Wu[a1], Hui Fu[a1], Xiaoye Zhou[c1], Lei Qian[a], Jiasi Luo[a], Jiaming Zhu[d], Wing Bun Lee[a], and Xu-Sheng Yang[a,b*]

[a]*State Key Laboratory of Ultra-precision Machining Technology, Department of Industrial and Systems Engineering, The Hong Kong Polytechnic University, Hung Hom, Kowloon, Hong Kong, China (E-mail: xsyang@polyu.edu.hk)*

[b]*Hong Kong Polytechnic University Shenzhen Research Institute, Shenzhen, China*

[c]*Guangdong Province Key Laboratory of Durability for Marine Civil Engineering, School of Civil Engineering, Shenzhen University, Shenzhen, Guangdong 518060, PR China*

[d]*School of Civil Engineering, Shandong University, Jinan 250061, China*

[1] These authors contributed equally to this work.

[*] Corresponding author. xsyang@polyu.edu.hk (X.-S Yang). Tel: +852-2766 6604

Abstract

Low-excess energy twin boundary can effectively stabilize the conventional grain boundary. It has been reported that deformation-activated nanotwins in nanograined metals produced by severe plastic deformation techniques can significantly enhance mechanical-thermal stability. However, fabrication, structural evolution and the effect of grain size and twin thickness on the mechanical stability of nanograined-nanotwinned metals, where both the grain size and twin thickness reach the nanometer scale (especially grain size is lower than 40 nm), remain unclear. In this study, a gradient nanostructured layer containing a nanograined-nanotwinned sub-layer region and an extremely refined twin-free nanograined top surface layer with grain size as small as ~ 10 nm is achieved on copper by using an ultrahigh-strain rate single point diamond turning technique. High-resolution transmission electron microscope observations, atomistic molecular dynamic simulations, and nanoindetation tests were performed to reveal the size-dependent mechanisms of grain refinement and hardness along the gradient direction. The propensity of deformation multifold twinning is increased firstly in large-size nanograins and then decreased once grain size is below ~ 48 nm, finally replaced by detwinning to form extremely fine twin-free nanograins at the topmost surface layer. In other words, both the zero-macrostrain-induced deformation multifold twinning and symmetry-breaking-based detwinning processes can continuously refine nanograins along the gradient direction. Critical grain sizes for deformation multifold twinning and detwinning are discussed. Interestingly, a Hall-Petch strengthening-softening transition is discovered at a critical grain size of ~30 nm in the gradient nanostructured layer. The softening mechanisms are elucidated to be attributed to the twin thickness effect on deformation mode in nanograined-nanotwinned structures and the pure grain boundary-mediated plasticity in extremely fine twin-free nanograins. A series of critical twin thicknesses for softening in nanograins with different grain sizes are discussed; that is, the smaller the grain size is, the smaller the critical twin thickness will be. This study offers the potential for understanding and developing stable nanostructured metals.

Keywords: Nanograined-nanotwinned Cu; ultra-precision machining technique; multifold twinning; strengthening-softening transition; high-resolution transition electron microscopy.

1 Introduction

"Smaller is stronger" is generally recognized following the empirical Hall-Petch effect. [1, 2]. Unfortunately, "smaller grain size, less stable" has also been proved in homogeneous nanograined (NG) metals by experiments and simulations [3]. On one hand, multiplication and motion of dislocations are severely inhibited in NG metals via significantly reduced grain size and increased density of grain boundaries (GBs), resulting in high strength but poor tensile ductility [4, 5]. On the other hand, grain coarsening and softening can be triggered in NG metals by mechanical and thermal stimulus, especially when the grain sizes are below certain critical values [6, 7]. This inherent instability of NG metals originates from the conventional GBs with high mobility. Interestingly, numerous investigations have indicated that the special twin boundary (TB) with obviously lower excess energy (usually smaller by an order of magnitude than the conventional GB) can effectively act as a thermally-mechanically stable interface for strengthening metals. For example, heterogeneous nanotwinned (NT) metals have shown the strengthening effects with comparable tensile uniform elongation [8-11]. In addition, ultra-hardness/strength and superior thermal stability have also been surprisingly discovered in nanograined-nanotwinned (NNT) materials, such as cubic boron nitride [12], diamond [13], Ni [14], and Ag-Cu alloy [15], etc., in which NGs (ranging from several to tens nanometers) contain thinner NTs. The relaxation of the GBs into lower-energy states by NTs has been proposed to increase the stability of NG metals under mechanical and/or thermally activations [6].

Similar to that in twin-free NG metals, a strengthening-softening transition has also been reported in NT metals once the twin thickness (λ) decreases below a critical value. For example, Lu et al. [16] reported the critical twin thickness is λ =15 nm in ultrafine-grained (UFG) Cu containing NTs, contributing to a maximum strength and then a strengthening-softening transition if λ is reduced. A series of critical twin thickness (λ = 12-37 nm) was also experimentally observed in UFG Cu (400-600 nm) [17]. More recently, experiments, simulations, and theories have been consistently to show that the critical twin thickness for the softening initiation depends on the grain size of metals; that is, the smaller the grain size d is, the smaller the critical twin thickness λ will be [15, 18, 19]. It implies that, in other words, the strengthening-softening transition would also happen in NNT metals. For instance, Ke et al. [15] successfully fabricated a series of NNT Cu-Ag specimens, observing the corresponding softening transition at critical twin thicknesses λ = 3.6-5.2 nm for the grain sizes d = 49-55 nm. Wang et al [18] reported statistically the critical values of λ and detailed deformation mode transition in NNT platinum (Pt) with various d and λ by in situ atomic-scale observations. In addition, atomistic molecular dynamics (MD) and theoretically modelling are also known to reveal the critical twin thicknesses and corresponding plastic deformation mechanisms for strengthening-softening transition behavior in NNT Cu [19]. To name a few, Zhu et al. [20] the large-scale MD simulations and quantitative continuum mechanism-based plasticity model to investigate the coupled effects of grain size and twin thickness on the strength and ductility of NT metals, predicting a critical twin thickness λ for the maximum strength is 13 nm when the grain size is 500 nm in NT Cu. Based on the twin thickness-dependent plasticity model, Wei [21] found that the critical twin thickness is proportional to square root of grain size for achieving the corresponding maximum strength. These twin-dependence on grain size activities may rise a question/challenge in NNT metals; that is, how to tailor the NTs (e.g. distribution and size) to persistently stabilize the GBs, especially for the multi-scale NGs (from several tens of nanometers to tens of nanometers).

Heterogeneous gradient nanostructured (GNS) metals (e.g. gradient phase, composition, and grain size) have been widely fabricated by various surface severe plastic deformation (SSPD) techniques. This type of structure can have the high strength-ductility by combining the strain/stress partitioning between the multi-scale domains along the gradient direction [22-24]. Noticeably, deformation twinning might be easily activated in low/medium-stacking fault energy (SFE) metals during the SSPD process. In this regard, the SSPD technique might be developed to achieve the stable gradient NNT structure (i.e., the twin thickness gradually reduces with decreasing grain size) by tailoring the morphologies of grain size and twin thickness simultaneously. For example, NNT structural regions were reported in GNS Ag, Cu, Ni and steel produced by SSPD techniques [6, 7, 25]. It was verified that the deformation NTs can stabilize the GBs by diminishing the mechanical loading-driven GB migration in the top surface region with the grain size between 40-75 nm in GNS Cu specimen, while the range of twin thickness was not considered [6]. However, it has been a challenge to experimentally verify the stability of TB-GB activities in smaller NGs due to the technological difficulty of synthesizing NNT materials. To date, the stability of TB activities of NG materials with $d \approx$ 10-20 nm was only be garnered by MD simulations [19]. More recently, Li et al [26] developed a two-step severe plastic deformation (SPD) process, i.e. SMGT and subsequent high-pressure torsion (HPT) in liquid nitrogen, obtained the extremely refined NGs that contained three-dimensional (3D) minimal-interface structures stabilized with TB networks. This special interfacial structure can effectively restrain the grain growth even near the melting point and exhibit an ultra-hardness close to the theoretical value. To the best of our knowledge, however, it is still quite limited literature to interrogate the structural evolution and stability of the extremely refined NGs in GNS metals produced by the single SSPD technique, especially the top surface region with the grain size d < 40 nm. This might be due to the technological difficulty in synthesizing by SSPD techniques, as the mechanical driven-grain coarsening and deformation detwinning would happen easily in NGs with too small grain sizes [23].

Increasing strain rate in the SPD process has been suggested to promote the dislocation multiplication and suppress the dislocation annihilation kinetics, thus effectively facilitating the grain refinement by forming more GBs or dislocation boundaries [27]. In this study, the single point diamond turning (SPDT), a high-speed ultraprecision surface machining method is developed to produce GNS Cu model material for achieving the extremely refined surface region. Cu is a medium SFE metal (~45 mJ/m^2) and known to form copious deformation NTs during the SPD process [28]. The ultra-precision SPDT technique in this work can achieve ultrahigh strain rate (up to 10^6 s^{-1}) with large strain (typically 2-10) on the workpiece, thus denoting many advantages, e.g. high efficiency and controllability, cost-effectiveness, and excellent surface quality [29]. Accordingly, the GNS Cu possessing both gradient NNT sub-layer region and extremely refined NG with grain size of ~ 10 nm at topmost surface layer is successfully prepared by the SPDT technique. Grain refinement process and related grain size-dependent plastic mechanisms of the SPDT-induced GNS layer, especially the NNT layer has been atomically explored by means of high-resolution transmission electron microscopy (HRTEM) observations and MD simulations. Noticeably, we confirm the twinning and detwinning of multifold NTs play a key role in the grain refinement process in NGs. Moreover, when the grain size is below 30 nm, a softening transition was observed. This softening mechanism is attributed to detwinning and twinning softening caused by the reduced grain size and twin thickness. Our results shed light on origin of softening transition in the fine NGs, which is critical to the development of mechanical stable nanostructured alloys.

2 Experiments and simulations

2.1 GNS layer fabricated by SPDT

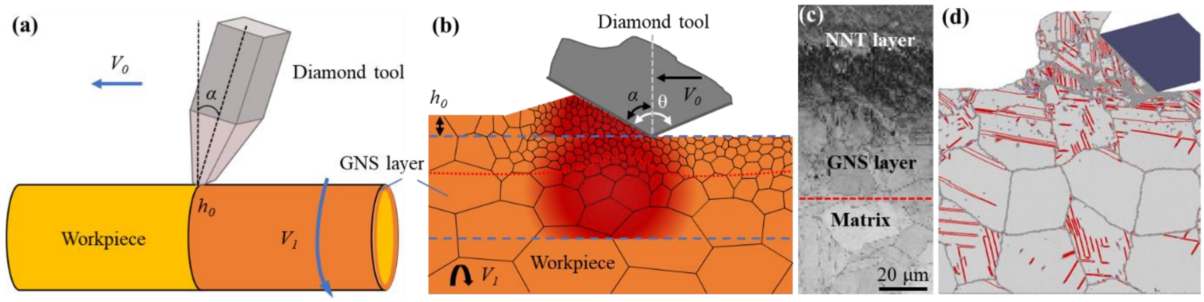

Fig. 1 (a) Schematic of SPDT technique. (b) Surface prow compression during the SPDT process. V_1, V_0, h_0 and α are the rotation velocity of the sample, the moving velocity of the diamond tool, the turning depth and the rake angle, respectively. (c) The cross-sectional SEM image of the SPDT Cu showing the formation of GNS layer. (d) MD simulation of SPDT process consistently showing the generation of GNS layer (atoms are colored by common neighbor analysis).

Commercial pure Cu (99.97 wt.%) rods consisting of well-annealed equiaxed coarse grains (CGs) (~23 μm) were first machined into cylindrical samples with length of 15 mm and diameter of 10 mm. The cylindrical workpieces were then subjected to SPDT treatment, as schematically shown in Fig. 1(a). As shown in Fig. 1(b), this high-speed machining process compress the deformation surface and thus result in gradient refinement, the detailed process described in Ref [30]. The high-speed SPDT parameters are listed as follows: cutting speed V_1 of 500 rpm, turning depth h_0 of 30 μm, rake angle α of 30° and feed rate V_0 of 5 mm/min, and the cooling media is paraffin lubricant. The SPDT process was repeated 20 passes to accumulate the SSPD effect for achieving a thick and uniform GNS layer.

2.2 Molecular dynamics simulations

In addition to the experiments, the MD simulations (Fig. 1(d)) by the LAMMPS software was assisted to understand of the formation of GNS Cu layer during the SPDT process. In particular, atomic microstructure evolution, especially the deformation twinning or/and detwinning mechanisms, will be dissected at the atomic level. The embedded-atom method (EAM) [31] was used to describe the interaction potential between Cu atoms. The simulated cell was built to have an average grain size of 24 nm and 10 nm in-plane and out-of-plane, respectively. After that, the model was first annealed to 700 K for 1 ns and then cooled down to 300 K in 0.3 ns, achieving the equilibrium status. A rigid body diamond quadrangular was modeled as the cutting tool. The cutting depth, cutting speed, cutting cycle and rake angle are 10 nm, 500 m/s and 30º and 10 cycles in this model.

2.3 Microstructure and mechanical properties characterizations

The longitudinal sections of the SPDT Cu samples were observed by scanning electron microscopy (SEM, TESCAM MIRA3). Electron backscatter imaging under SEM was used to investigate the microstructure of the GNS layer. The SEM specimens were prepared via both mechanical polishing and vibration polishing. The plane-view TEM observations were performed using the field emission JEM-2100F at 200 kV. The TEM samples were taken at different depth of the GNS layer by mechanically polishing. Then, mechanically polish was continued from the side away from the observation layer, obtaining the ~25 μm-thick TEM slices. Then, the TEM slices were further thinned on the Gatan 691 precision ion polishing system through the single-side ion milling mode.

The nanoindentation tests along the depth direction of the SPDT samples were conducted on a Hysitron TI-900 Triboindentor. The max load and holding time are 8 mN and 5 s, respectively. The loading rate and unloaded rate is the same, 0.4 mN/s. The nanoindentation test was repeated 10 times at each sample.

3 Results

3.1 Grain refinement in GNS layer during the SPDT process

The cross-sectional image of the SPDT Cu sample characterized by SEM is shown in Fig. 1(c). It shows that a GNS surface layer with a depth of ~80 μm is successfully prepared. Due to the intensive plastic deformation and refined NGs near the top surface layer, GBs are difficult to identify in this region compared with that of the matrix region. Therefore, detailed HRTEM characterizations at various depth layers along the gradient direction has been carried out to uncover the underlying grain refinement mechanism in GNS layer, where two characteristic regions are defined according to the grain size range. The first one is the deformed sub-layer region deeper than ~20 μm, where the grain size ranges from tens of microns to hundreds of nanometers, and grain refinement is primarily achieved via full dislocation activities. The second one is the NNT region between ~20 μm depth and topmost surface layer, where the grain sizes refine from ~100 nm to ~10 nm. Detailed microstructural evolution for the grain refinement processes in these two regions are described as follows.

3.1.1 Grain refinement in the deformed sub-surface region

Fig. 2(a-d) presents a series of TEM bright-field (BF) images taken from deformed sub-surface layer region deeper than ~20 μm. Fig. 2(a) is the BF TEM image in the region ~ 60 μm depth, near the strain-free matrix, which the grain size is smaller than ~10 μm. High-density dislocations (labelled as yellow triangles) are generated by plastic deformation as shown in Fig. 2(a). When the depth reaches ~ 40 μm, the grain size is refined to several micrometers, as shown in Fig. 2(b), in which lamellar structures/sub-grains (labelled as red arrows) are formed to contain large dislocation clusters, dislocation walls and dislocation cells. Furthermore, a typical microstructure of the 25 μm-depth region is presented in Fig. 2(c). The equiaxed UFGs with grain size down to several hundreds of nanometers are formed, and dislocation clusters can be found in the interior of these UFGs. Noticeably, deformation twins with average λ about tens of nanometers are started to be found in some UFGs in this depth layer, as shown in Fig. 2(d) and corresponding inset. Fig. 2(d)-(e) also show that numerous inclined perfect dislocations are accumulated to cut through TBs, as evidenced by Fourier filtered images in Fig. 2(f-g). Dislocations piled up at $\Sigma3\{111\}$ TBs may result in the formation of large-angle GBs by gradually losing the coherency, thus leading to the further refinement of NTs into NGs. This refinement mechanism has been verified in SPD Cu [32].

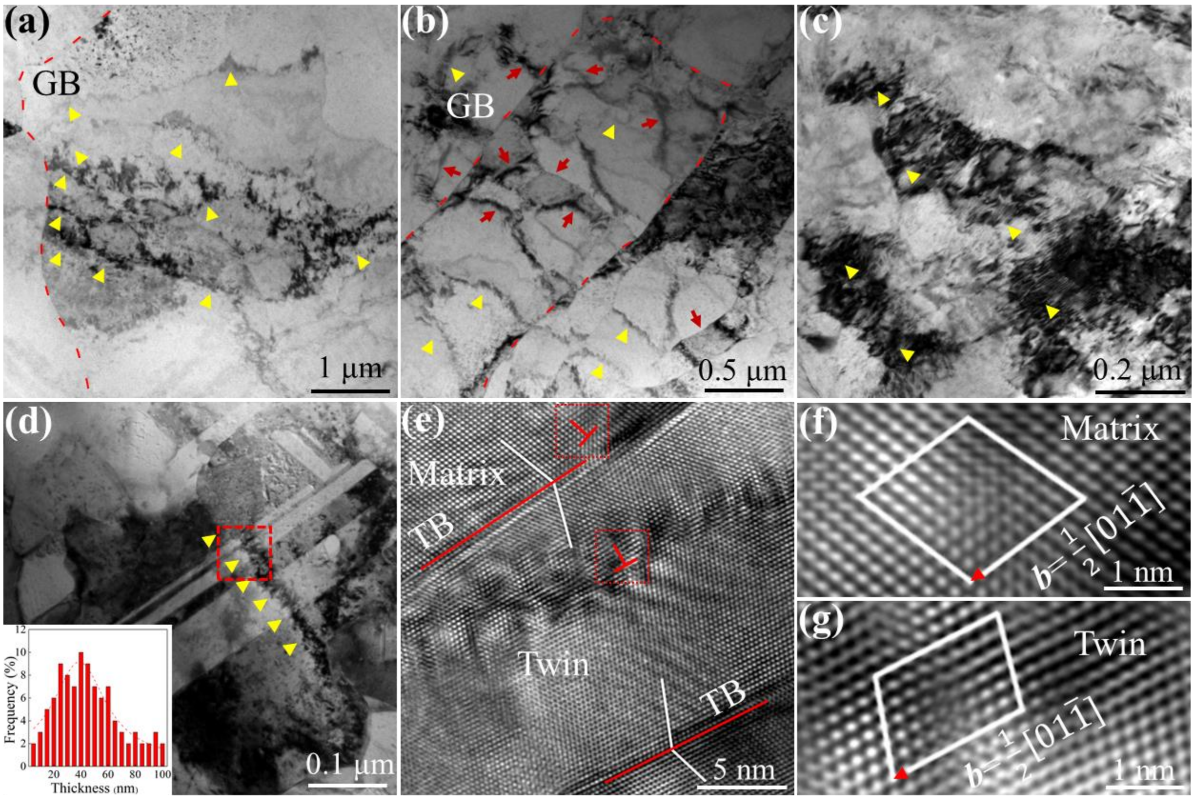

Fig. 2 Detailed microstructural evolution of the deformed sub-surface region deeper than~20 μm. Typical BF TEM images showing the microstructures at different depths: (a) ~60 μm, (b) ~40 μm, (c) ~25 μm. (d) TEM image showing the deformation twins in the region of ~25 μm depth, where the inset gives the twin thickness distribution. (e) HRTEM image of T/M lamellar taken from the region outlined in (d). (e-f) Corresponding Fourier-filtered images of perfect dislocations in matrix and twin, respectively.

3.1.2 Grain refinement in the gradient NNT region

TEM images for the detailed microstructures across the depth span of 0-20 μm in the GNS layer are given in Fig. 3(a-e), showing the equiaxed NGs with random crystallographic orientations and gradient grain size. It is noted that dense deformation NTs including multifold NTs (marked by yellow arrows) are found to embed in these NGs, thereby forming a gradient NNT structural region. Different from the NTs in UFGs, the λ values of NTs in these NNT grains are significantly thinner (below 10 nm) and keeps dropping with decreasing d. However, the twin fraction (φ) is increased first and then decreased with decreasing d as shown in Fig. 3(f). For example, the value of φ is ~17.4% at depth of ~20 μm (d ≈ 88 nm), which is increased to the peak about 32.6% at depth of ~15 μm (d ≈ 47.6 nm), and subsequently decreased to be only ~2.5% at depth of ~15 μm (d ≈ 10.5 nm). Lastly, NTs are hardly observed in the topmost surface (d ≈ 10 nm), as shown in Fig. 3(e).

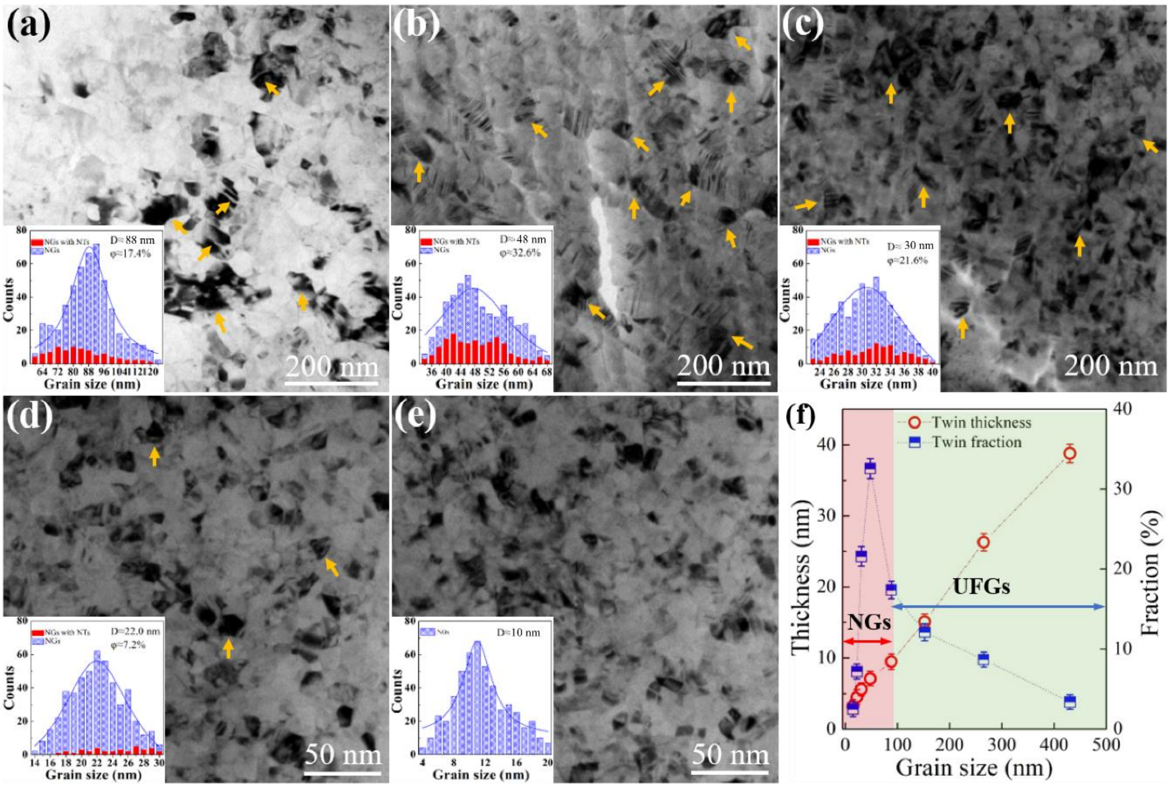

Fig. 3 Detailed microstructural evolution of the gradient NNT region across the depth span of 0-20 μm. Typical TEM images at different depth layers: (a) ~20 μm depth. (b) ~15 μm depth. (c) ~10 μm depth. (d) ~5 μm depth. (e) Topmost surface. Insets are the size statistics of the NGs and the corresponding fraction of NGs contained deformation NTs. (f) Statistical diagram of twin thickness and twin fraction dependence on grain size in GNS Cu.

The above microstructural evolution observations evidence that a gradient NNT region with extremely refined NGs ($d \approx 10$ nm) in the topmost surface has been successfully achieved in GNS Cu by the SPDT technique. It is no doubt that deformation twinning can effectively refine the UFGs into the NGs. However, it is noted that the deformation twinning becomes more difficult when the grain size refines too small. Therefore, one may ask why NGs can be continuously refined with the decrease of the fraction of deformation NTs. It may be related to the existence of deformation multifold NTs [33, 34]. In contrast to the conventional NT metals with parallel TBs, multifold NTs in NGs contain the intersectant TBs, which is similar with the hierarchical NTs [35, 36]. Relative to the parallel NTs, on one hand, multifold and hierarchical NTs with different orientations are more effective in refining the grain, due to the enhanced TB-dislocation interactions [35, 36]. On the other hand, excess dislocations pile up in TBs would lead to the symmetry-forming and -breaking processes of multifold NTs, which play a crucial role in the further grain refinement process of NGs [37, 38]. The formation mechanisms and corresponding grain refinement function of multifold NTs will be dissected by the HRTEM observations and MD simulations.

3.2 HRTEM characterization for deformation multifold NTs in NGs

HRTEM observations were conducted to atomic-level characterize the deformation multifold NTs in NGs with different grain sizes in NNT region. Fig. 4 is the typical HRTEM image of NG (d ≈80 nm) which contained various kinds of deformation multifold NTs (including 2-F, 3-F, and 5-F NTs). It is noted that the parallel NTs and crossed multifold NTs are coexisted in NG. These deformation NTs prefer to nucleate and grow via Shockley partial dislocations emission from GBs. As marked by white arrows in Fig. 4(a), dense SFs are also resulted from the emission of the Shockley partial dislocations from GBs. Fig. 4(b) presents the enlarged image in upper region of the NG in Fig. 4(a). The NTs originated from the left (TB1) and top (TB5) boundaries of the NG are intersected to form 2-F NT, while the 3-F NT is formed by intersecting NTs from the left (TB1), right (TB4) and top (TB5) boundaries. In addition to the SFs along the TBs, $\sum 3\{112\}$ incoherent TBs (ITBs) are found to link with intersection nodes or incomplete multifold NTs, as indicated by green arrows in Fig. 4(b). Specifically, $\sum 3\{112\}$ ITBs may have the 9R phase structures, as evidenced by the extra diffraction spots with three times interplanar spacing of Cu {111} from the fast Fourier transform (FFT) patterns inserted in Fig. 4(b). The 9R phase structure with stacking order of BCBCACABA is also well-indexed in Fourier-filtered atomic image for 2-F ITB region enlarged in Fig. 4(c). Previous report has verified that deformation twinning in NG metals can be accomplished by the migration of 9R $\sum 3\{112\}$ ITBs by cooperative passage of a repeatable sequence $\boldsymbol{b_1}$:$\boldsymbol{b_2}$:$\boldsymbol{b_3}$ Shockley partial dislocations on every (111) plane [39]. In contrast to the common deformation twinning in CG and UFG regimes, this twinning mechanism in NG regime yields zero-net macrostrain because the sum of their Burgers vectors equal zero. In other words, the 9R structural $\sum 3\{112\}$ ITBs can also provide the nucleation sites to form deformation multifold NTs in NGs, which is similar to the role of GBs in NGs [33]. The Fourier-filtered image of 3-F NT shows twin pole migration in Fig. 4(d). For this 3-F NT, the intersection acute angles between TB1 and TB5, TB5 and TB4 are 76.04° and 70.20°, respectively. In addition, TB migration is observed in this 3-F NT, where TB4 migrates to form a seven atomic-layers twin lamella.

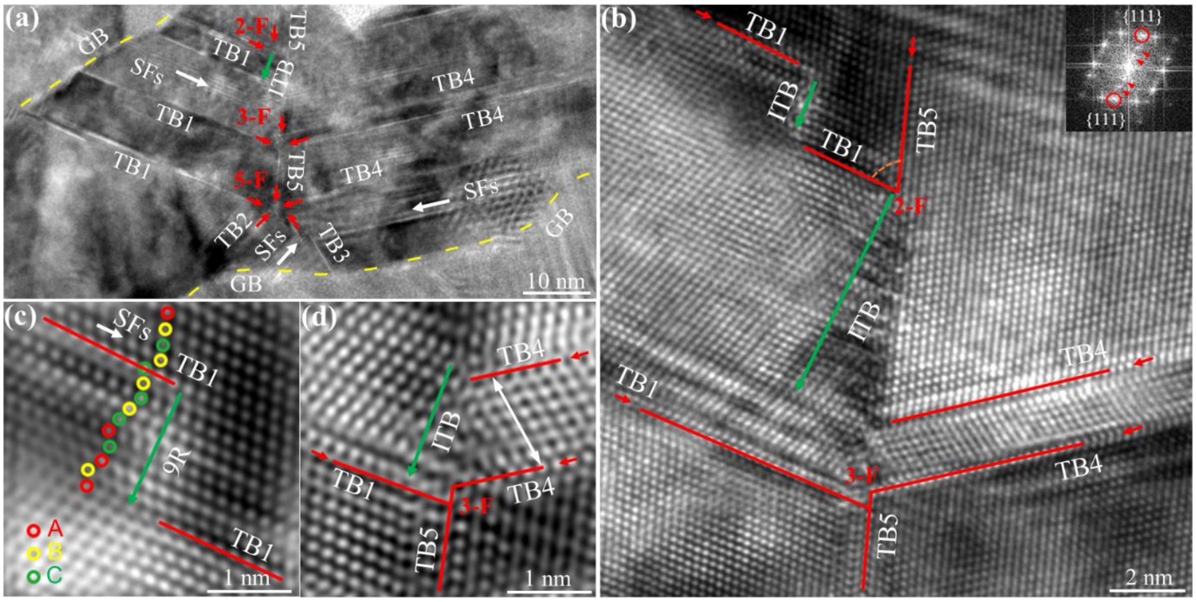

Fig. 4 (a) HRTEM image of the deformation multifold NTs in NG with grain size of ~ 80 nm. Yellow dash line represents GB, while red, green and white arrows represent TB, ITB and SFs, respectively. Twofold, threefold, fourfold and fivefold NTs are abbreviated as 2-F, 3-F, 4-F and 5-F, respectively. (b) Enlarged image for 2-F and 3-F NTs in (a). (c-d) Corresponding Fourier-filtered atomic images of ITBs and 3-F NTs, respectively.

Fig. 5(a-b) give the HRTEM images about the deformation multifold NTs in two typical NGs with $d \approx 20$ nm in the NNT region. In comparison with that in the relatively larger NGs, there are also some ITBs formed at the intersection nodes by the parallel and crossed multifold NTs, as shown in Fig.5 (a). However, no 9R structural $\sum 3\{112\}$ ITBs are obviously observed to assist the deformation multifold NTs in the smaller NGs. This might be due to that the large area for forming the 9R structure cannot be provided sufficiently when decreasing the grain sizes of NGs. Alternatively, synergy-pole twinning mechanism would dominate the deformation multifold NTs process in the smaller NGs. Specifically, each TB would be formed by the random activation of partials (RAP) emitted from GBs, which has three Shockley partials with equal numbers and also yield a zero-net macrostrain [40]. It is evidenced by the smooth GB segments that intersect with the TBs (Fig. 5(a-b)). For example, complete 3-F, 4-F, and 5-F NTs in Fig. 5(a) should be formed by intersection of three, four and five single NTs, respectively, all of which would be formed by the RAP emitted form GBs. The transition between these two zero-macrostrain 9R and RAP deformation twinning mechanisms has also been reported in NG Cu with reduction in grain size in NNT region [41]. Noticeably, a twinning pole splitting and TB migration of TB4 are observed for 5-F NT in another smaller NG, resulting in the symmetry breaking of the deformation multifold NTs and releasing of intersectant CTBs self-locking state as shown in Fig. 5(c). In addition, there exist successive steps in the TB4 (Fig. 5(d)), where the four atomic-layer step leads to the migration and detwinning of TB4 towards GB. TB Combined with the statistical analysis in the decrease of NTs in Fig. 3, the twin pole splitting/migration (Fig. 5(c)), TB migration (Fig. 4(d))and steps (Fig. 5(d) would be incorporated to induce the detwinning process with the reduced grain sizes of NGs in NNT region [37].

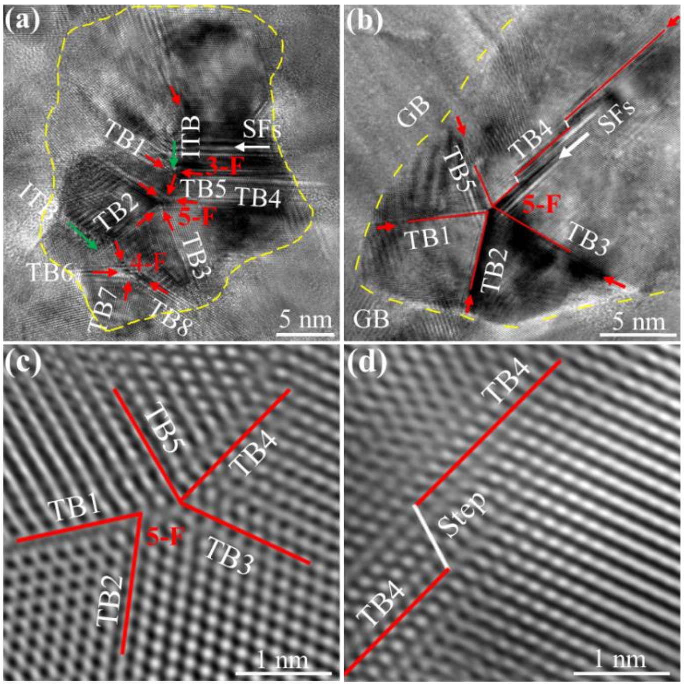

Fig. 5 (a-b) HRTEM images of the deformation multifold NTs in two typical NGs with grain sizes of ~ 20 nm. Fourier-filtered atomic image of 5-F NTs (c) and step (d) enlarged from (b).

Fig. 6(a) presents the typical TEM image of the NG with d≈16 nm. Only twofold NT (marked as TB1 and TB2) is found in this grain. Crossed twin interfaces with an angle of ~109° between TB1 and TB2 are shown in Fig. 6(b). The node of this twofold NT lies on the GB and the node is also linked with the ITBs. In addition, the TB1 is broadened by tens of atomic-layer migration. Considering the higher stability of twofold NT among the multifold NTs, it can be inferred that the occurrence of this twofold is caused by the detwinning process of multifold

NTs [42]. In addition, the migration of the twin pole from grain interior to GBs as well as TBs broadening indicate the detwinning process is overwhelming in NGs with reduced grain sizes. This result is consistent with the results from Fig. 3(f) that the number of NTs is significantly decreased when the grain sizes reduce to tens of nanometers. At last, there are no NTs observed interior of the grain when then grain size reduces to ~12 nm as shown in Fig. 6(c). From the Fourier-filtered image as shown in Fig. 6(d), one can see that the closely packed {111} planes of grain interior are inclined by 6.4° to that of grain outside. It can be inferred that a deformation mode transition from deformation twining/detwinning to GB mediated-plasticity when the grain size is below 12 nm.

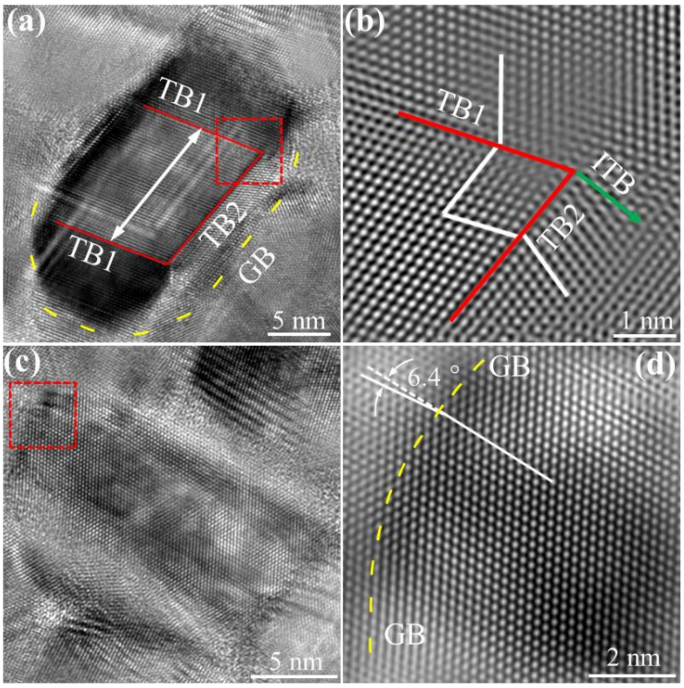

Fig. 6 (a) Typical HRTEM image of the twofold NTs in NG (d≈16 nm) and (b) related Fourier-filtered image of pole. (c) Typical HRTEM image of NG (d≈12 nm) and (d) related Fourier-filtered image of GBs.

3.3 Strengthening-softening transition in GNS layer

According to the microstructure observations and nanoindentation tests, Fig. 7(a) summarizes the varying average grain size, twin thickness and hardness along the depth direction from the top surface to undeformed matrix in the SPDT Cu sample. It shows that the average grain size is gradually refined from ~23 μm in the matrix region (depth of ~ 80 μm) to ~10 nm in the top surface layer. Correspondingly, the twin thickness is also reduced from ~38.8 nm (depth of ~ 25 μm) to ~3.2 nm (depth of ~ 2 μm). However, corresponding hardness is firstly increased from ~ 0.95 GPa in the matrix to a maximum value of ~ 2.76 GPa at the ~10 μm-depth layer (d~ 30 nm), which is then gradually reduced to 2.58 GPa at the topmost surface layer. Obviously, there is a strengthening-softening transition in the GNS layer. Fig. 7(b) displays the Hall-Petch plot with the hardness as a function of $d^{-1/2}$ along the gradient direction in the NNT region of the SPDT Cu, in which the corresponding twin thickness is also given. Consistently, the measured hardness in Fig. 7(b) initially follows a traditional positive Hall-Petch relationship, achieving a peak point (~ 2.76 GPa) at a critical grain size of ~ 30 nm. After that, such a relationship is broken down when d < ~30 nm, namely, a negative Hall-Petch slope with the sign of softening. Note that concurrently gradient reduction in the sizes of GBs and TBs might lead to the cooperative strengthening effects in the Hall-Petch relationship. Therefore, the hardness achieved in the NNT layer in our SPDT Cu in Fig. 7(b) surpasses the hardness reported from some referenced nanostructured Cu, such as NT Cu prepared by pulsed electrodeposition (PEP) [11]. In addition, there have been several experimental reports about grain size softening [43, 44] and hardening [45-48] when the grain sizes reduce to tens of nanometers.

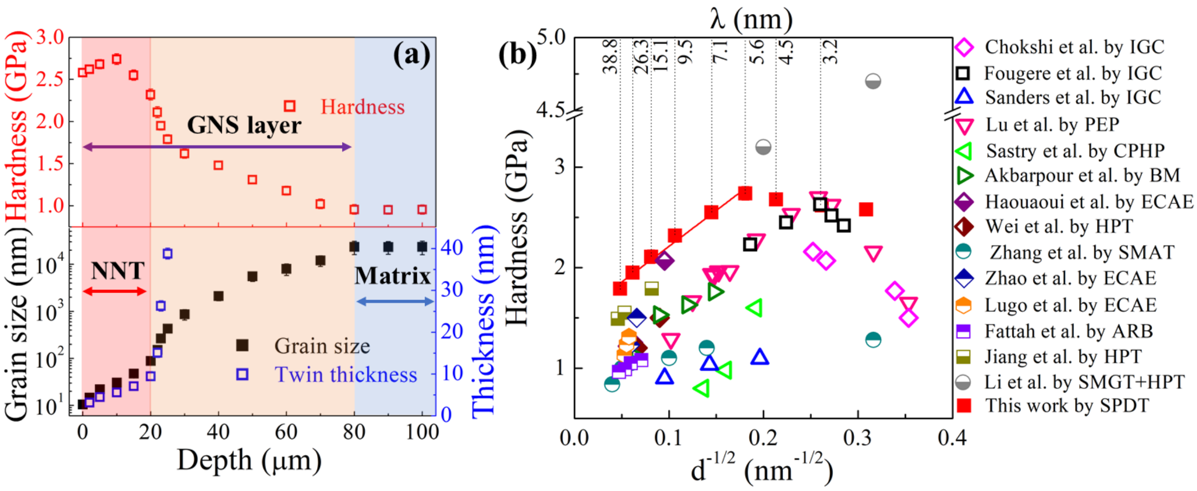

Fig. 7 (a) Variation of average grain size, twin thickness and hardness along the depth direction from the treated top surface to unformed matrix in the SPDT Cu sample. (b) Hall-Petch plot in the NNT region of SPDT Cu. The hardness values (H) from some literature are calculated from yield strength (σ_y) by Tabor relation, i.e., $\sigma_y \approx$ H/3 [49].

Some experimentally data of Cu from literature is added in Fig. 7(b) for comparison [16, 43-48, 50-55]. Hall-Petch softening behaviors have been normally observed in NG Cu prepared by some bottom-up methods, such as Inert gas condensation (IGC), ball milling (BM), cold pressing and hot pressing (CPHP) shown in Fig. 7(b). However, it has been suggested that the incomplete densification-induced residual porosity during the above fabrication methods may result in the poor bonding between particles and thus be responsible for the softening. In contrast, conventional SPD methods, including accumulative roll bonding (ARB), equal-channel angular extrusion (ECAE) and HPT, etc., are hard to achieve NGs with grain sizes down to tens nanometers for checking the availability of the strengthening-softening transition. If only increasing the plastic strain during these SPD processes, grain coarsening-induced softening would happen frequently, rather than the continual grain refinement [23]. Surprisingly, SMGT and HPT were recently developed to prepare several nanometer-sized NG Cu with 3D minimal-interface structures stabilized by TB networks [26]. This NNT structure can suppress the grain coarsening and exhibit an ultra-hardness, as shown in Fig. 7(b), in lieu of the softening transition. By employing the SPDT technique with a high strain rate, for the first time, we report the strengthening-softening transition involved in the GNS NNT Cu layer with continual grain refinement to ~ 10 nm-grain size at the topmost surface.

4 Discussion

The above experimental results indicate that a high-speed SPDT technique has been validated to successfully fabricate a gradient GNS Cu layer, in which grain size is continually and significantly refined to ~10 nm at the topmost surface layer. Noticeably, a gradient NNT surface region across the depth of ~20 μm is refined by two main plastic mechanisms, i.e., gradually transiting from multifold twinning-dominated plasticity in UFGs and relatively larger NGs to multifold detwinning-mediated plasticity in relatively smaller NGs once $d < \sim 48$ nm along the gradient direction. Accordingly, a strengthening-softening transition is confirmed at a critical d of ~30 nm. Thus, three critical issues, i.e., (i) grain size effect on the twinning and detwinning of multifold NTs, (ii) their atomic movement mechanisms in grain refinement processes, and (iii) strengthening-softening transition mechanisms in NNT region, will be systematically discussed in this section.

4.1 Grain size effect on the multifold twinning and detwinning in NNT region

Consistent with numerous experiment and simulation results, our observations have testified that the deformation NTs in NGs are corresponding to the partial dislocations emitted from GBs [56-58]. During the high-strain rate SPDT process, the stress for a twinning partial dislocation nucleation, τ_p, can be expressed as [28, 59]:

$$\tau_p = \frac{2\alpha G\boldsymbol{b_p}}{d} + \frac{\gamma}{b_p} \tag{1}$$

where α is the dislocation parameter (i.e. edge dislocations with $\alpha = 0.5$, while $\alpha = 1.5$ for screw ones [60]) representing the scaling factor between the dislocation source length and grain size, G is the shear modulus of Cu (54.6 GPa[61]), γ is the SFE of Cu (45 mJ/m^2 [61]), $\boldsymbol{b_P}$ is the Burgers vector of partial dislocation, and d is the grain size. If consider the localized stress concentration for the activation of deformation twinning, Eq. (1) can be described as [62]:

$$n \cdot \tau_p = \frac{2\alpha G\boldsymbol{b_p}}{d} + \frac{\gamma}{b_p} \tag{2}$$

where n is a stress concentration factor. In addition, the stress required to trigger the perfect dislocation is:

$$\tau_N = \frac{2\alpha G\boldsymbol{b_N}}{d} \tag{3}$$

where $\boldsymbol{b_N}$ is the Burgers vector of perfect dislocation. For Cu, $\boldsymbol{b_P}$ and $\boldsymbol{b_N}$ are 0.148 nm and 0.256 nm, respectively. According to Eq. (2) and (3), there exists a critical grain size d_C, below which the stress for the activation of the partial dislocations is lower than that of perfect dislocations

$$d_C = \frac{2\alpha G(n\boldsymbol{b_N} - \boldsymbol{b_P})\boldsymbol{b_P}}{\gamma} \tag{4}$$

Accordingly, d_C is determined as ~131 nm. As a result, deformation twinning caused by partial dislocation emission tends to trigger when d < ~ 131 nm in Cu. These predictions are verified by our experiments results, i.e., multifold NTs domain the grain refinement when grain size lower than one hundred nanometers, as shown in Fig. 3.

In contrast to the twinning process, the detwinning process might be happened via the TB migration by the trailing partial dislocations gliding. Therefore, a simplified equation has been proposed to evaluate the optimum grain size (d_m) for deformation NTs, which can be written as [61]:

$$\frac{d_m}{\ln(\sqrt{2}d_m/a)} = \frac{9.69 - \upsilon}{253.66(1-\upsilon)}\frac{Ga^2}{\gamma} \tag{5}$$

where v and a is the Poisson's ratio and lattice parameter, respectively. The calculated d_m for deformation NTs in Cu is ~ 46 nm [61]. This d_m value is consistent with the size of the NGs (~ 48 nm) with the most profuse NTs in NNT region. When the grain size is smaller than d_m, twinning will be suppressed and detwinning will be overwhelming in NGs along the gradient direction.

4.2 Atomic mechanisms of multifold twinning and detwinning in NNT region

According to HRTEM observations in Fig. 4-6, we have identified the zero-macrostrain multifold twinning mechanisms, either through the immigration of 9R structural ITBs by cooperative activation of partials or RAP from GBs. Meanwhile, multifold detwinning process dominated by symmetry breaking, including twin pole splitting/migration and TB migration, is proposed to realize the further grain refinement. In addition, the grain refinement process by multifold twinning and detwinning is also observed during the atomistic MD simulated SPDT process. Herein, we dissect the dynamic atomic-scale microstructural evolution of representative 5-F NT twinning and detwinning processes to unveil the atomic mechanisms of multifold twinning and detwinning.

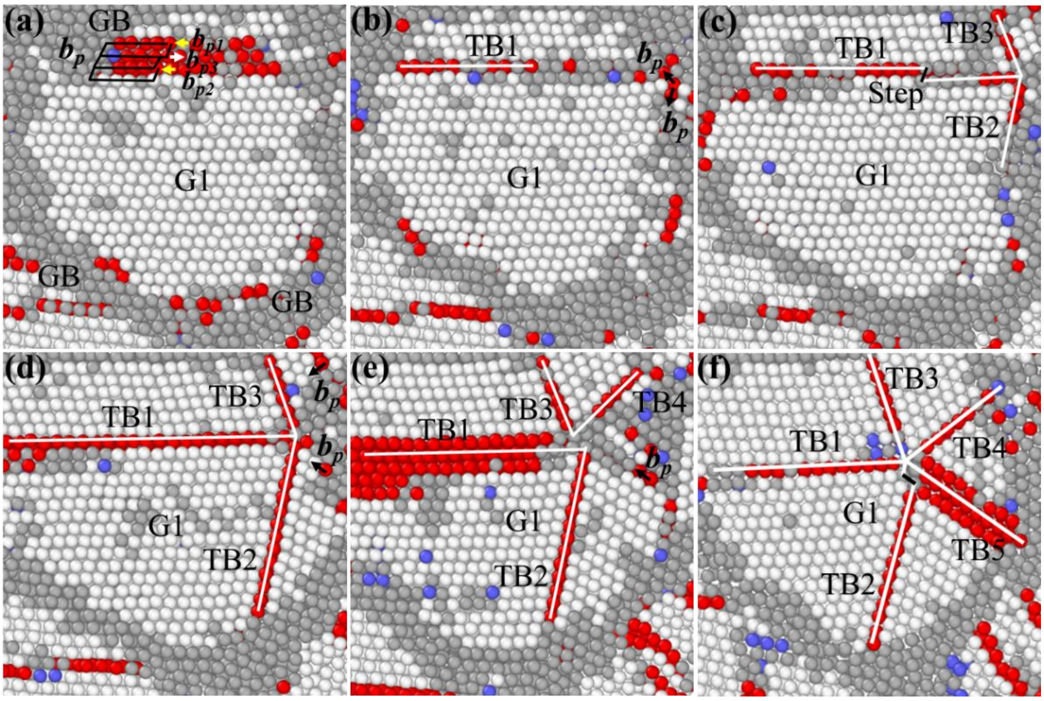

Fig. 8 MD simulated twinning process of 5-F NT. (a) The initial NG G1 without NTs inside. (b-f) Dynamic twinning process showing that TB1, TB2, TB3, TB4, and TBs are all formed by partials nucleation from GBs.

Fig. 8 shows a series of atomic-scale images to present the microstructure evolution of a 5-F NT formation during the simulated SPDT process. At first, several partials are found in Fig. 8(a) to nucleate and emit from GB of one NG, which is labeled as G1 under projection zone

[110]. Three Shockley partials with Burgers vectors of $\mathbf{b}_{p1}= \frac{1}{6}[\bar{1}2\bar{1}]$, $\mathbf{b}_{p2}= \frac{1}{6}[2\bar{1}\bar{1}]$, and $\mathbf{b}_{p3}= \frac{1}{6}[\bar{1}\bar{1}2]$ can be indexed to slip on three consecutive (111) planes, which apparently generate a total $\boldsymbol{b}$ of zero. This is a typical zero-macrostrain RAP twinning mechanism, as no deformation affecting the neighboring lattice structures, which is consistent with the experiment results. The zero-macrostrain RAP twinning grows laterally along with the three layers of the {111} planes in grain G1, resulting in the formation of short TB1, as shown in Fig. 8(b). In addition, some partials are also emitted from GBs for forming TB2 and TB3, which are verified in the subsequent Fig. 8(c). A typical 2-F twin is formed with intersectant TB2 and TB3. Then TB1 extends with steps to become 3-F twins as shown in Fig. 8(c). The TB2 and TB3 are both extended, and the pole of 3-F twin is migrated from the periphery of the grain to the center. In addition, some partials are ready for TB4 and TB5 in the GBs as shown in Fig. 8(d). TB4 is formed and jointed to 3-F twin to become the 4-F twin. The pole of 4-F twin further migrates to the center of the grain as shown in Fig. 8(e). Finally, TB5 is formed and jointed to 4-F twin to become the 5-F twin. The pole of the 5-F twin is near the center of the grain. As a result, our simulated results successfully verify the zero-macrostrain multifold twinning mechanism.

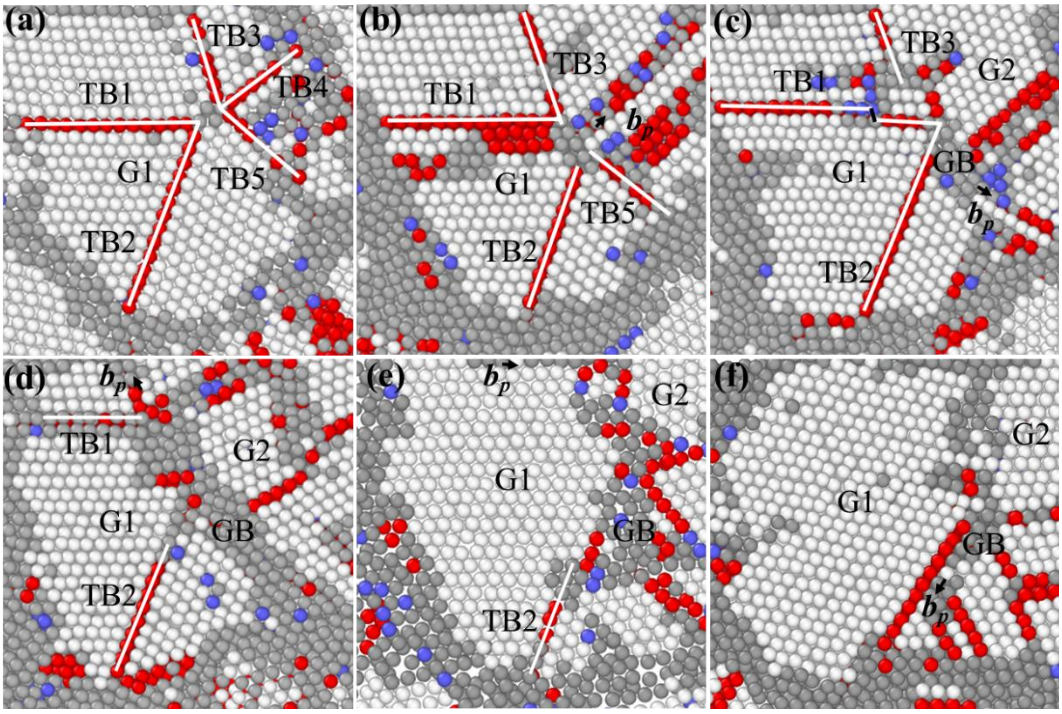

Fig. 9 MD simulated detwinning process of 5-F NT. (a) The pole splitting of NG G1 including the 5-F twin. (b) The grain G1 includes the fourfold twin. (c) The grain G1 includes the threefold twin. (d) The grain G1 includes the twofold twin. (e) The grain G1 includes the single twin. (f) The grain G1 without twins inside.

Besides, Fig. 9 presents successive images to show the detwinning process of a 5-F NT inside a NG labeled as G1. Firstly, the symmetry of 5-F NT is initially broken by the pole splitting as shown in Fig. 9(a). The 5-F NT is consequently divided into two regions, i.e., a 2-F NT (TB1 and TB2) and a 3-F (TB3, TB4 and TB5) NT regions, respectively. Then, TB4 is transformed by TB migration and partial dislocation slipping is detected accordingly, as shown in Fig. 9(b), forming two 2-F NTs. It implies that the 2-F NTs are more stable in relatively smaller NGs, in comparison with higher multifold NTs in relatively larger NGs, which is consistent with the experiment results. Subsequently, the detwinning process of two 2-F NTs is continued (Fig. 9(c-d)). To be specific, TB5 and TB3 are both shrunk significantly and gradually transformed to one conventional GBs by partial dislocation slipping to form a new grain G2. Finally, TB1 and TB2 are further migrated and integrated to a GB by partial dislocation slipping, eliminating the TB inside of G1. As a result, the multifold detwinning process can further refine the original G1 into two NGs (i.e., G1 and G2) with smaller gain sizes, which is consistent with our experiment results.

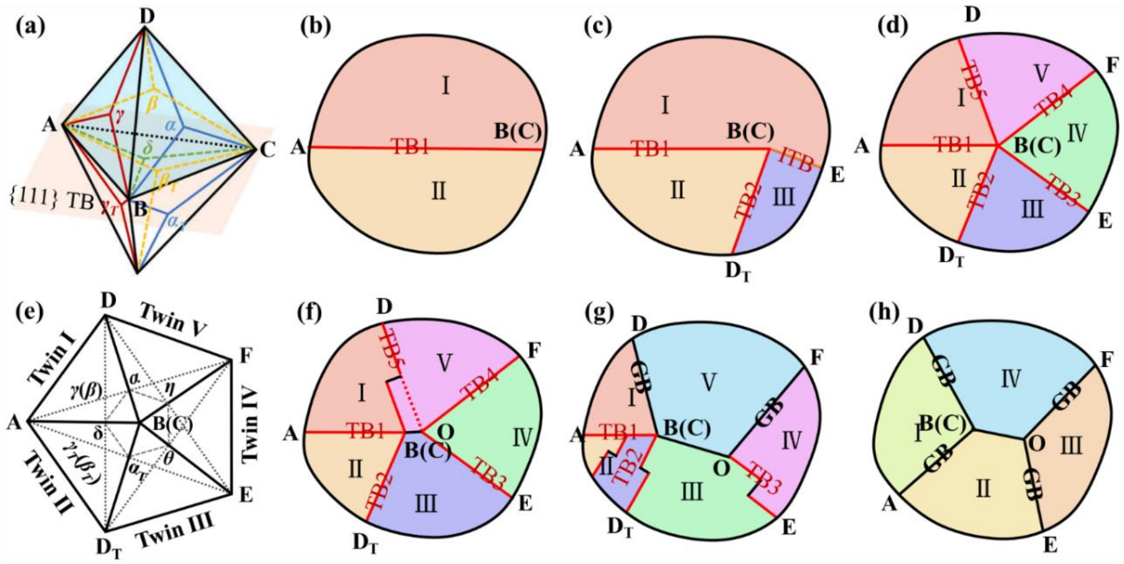

Fig. 10 (a) Illustration of the double FCC Thompson tetrahedron. (b)-(d) Schematic illustration of formation process of multifold NT. (e) Thompson tetrahedron Relationship in 5-F twins. (f)-(h) Schematic illustration of detwinning process of multifold NT.

A double FCC Thompson tetrahedron is used to uncover the twinning and detwinning mechanisms of multifold NTs as shown in Fig. 10(a). Vertex-to-vertex, vertex-to-orthocenter and orthocenter to-orthocenter represent perfect dislocation, partial dislocation and stair-rod dislocation, respectively [63]. Based on experiment and MD results, the 5-F twin units are corresponding to five adjoining Thompson tetrahedrons as shown in Fig. 10(a) and (e). On one hand, the formation mechanism of multifold NTs is attributed to the partial dislocation nucleating and slipping from GBs. The first step is the formation of a simple twin (ABC) with domains I and II via partial dislocation emissions from GBs under applied external stress action as shown in Fig. 10(b). The variation in stress orientation can also activate another partial emitted from the GB to nucleate a new twin (BCD_T), forming a twin domain III and an ITB, which effectively converts the regular twin in Fig. 10(b) into a 2-F twin as shown in Fig. 10(c). Note that ITBs also can provide the twinning dislocations for the nucleation of the multifold NTs. Under varying stress orientations, several partials with various glide directions to be activated sequentially to finally form the 3-F, 4-F and 5-F, respectively.

On the other hand, the symmetry-breaking mechanism dominates the detwinning process of the multifold NT for the further grain refinement in our work. It includes symmetry-breaking twin morphology (TBs migration, twin pole splitting and migration). Fig. 10(f) schematically illustrates that the detwinning process is related with the TB5 migration. The partial dislocation is nucleated near the TB1 and then glides along TB1 away from the twin pole. The continuous TBs migration induces the twin pole migration along TB1. As a result, symmetric twin pole B(C) migration is completed by partial dislocations slipping. Moreover, the partial dislocation slipping or step on TB2 leads to a several-layer migration of TB2 as shown in Fig. 10(c). Then the partial dislocations and the stair-rod dislocations dissociated from the random partial dislocations on the curved TB2 induce to further symmetry-breaking of twin pole. Moreover, with further TBs migration and twin pole splitting, new conventional GBs can be formed from TBs though partials activities-mediated grain rotation, leading to the grain refinement.

4.3 Strengthening-softening transition mechanism in NNT region

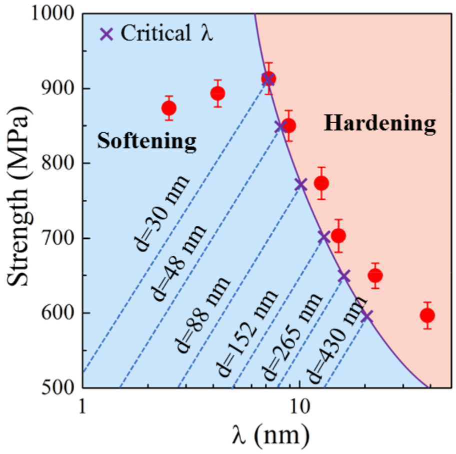

Fig. 11 Yield stress of NNT region as a function of twin thickness for different grain sizes.

Combined with the statistical TEM data and nanoindentation tests, deformation NTs present a clear size effect on the strengthening-softening transition in the NNT region. On one hand, the detwinning occurs when the grain size is down to ~ 48 nm. The detwinning process exhibits the strain relaxation of TBs. Several types of theoretical models have been developed to predict the critical thickness for the strengthening-softening transition in NT metals. For example, a dislocation-based theoretical model was developed by incorporating the functions of densities of dislocations pile-up zones of TBs (including primary and secondary twin lamellae) and GBs to describe the twin thickness and grain size-dependent flow stress of hierarchical NT metals [20, 64], thus yielding the critical values for the strengthening-softening transition. It should be noted that the intersection effect of multifold TBs and partial dislocations is hardly to quantitatively evaluate. On the other hand, a dislocation nucleation-based model has been proposed to describe the dependence of material strength (σ) on twin thickness and grain size in the following equation [19]:

$$\sigma = \frac{\Delta U}{SV^*} - \frac{k_B T}{SV^*} \ln\left(\frac{d}{\lambda}\frac{V_D}{\dot{\varepsilon}}\right) \tag{6}$$

The first component in the right side of Eq. (6) can be regarded as the athermal shear resistance and the second component is due to thermal softening. Accordingly, the critical λ for the strengthening-softening transition in the present work can be directly derived from the intersection points of the yield stress versus λ curve and the measured Hall-Petch curve at different grain sizes. More specifically, ΔU, S, V^*, k_B, T, V_D and $\dot{\varepsilon}$ are the activation energy, factor related to local stress concentration and geometry, activation volume, Boltzmann constant, temperature, Debye frequency ($1.3\times10^{13}s^{-1}$), and macroscopic strain rate, respectively. According to previous experimental studies, k_BT/SV^* is about 200 MPa, The corresponding athermal shear resistance is near the ideal shear strength as ~G/10 (G = 54.6 GPa for Cu [19]). In our experiment, $\dot{\varepsilon}$ is ~4.6×10^5 s^{-1}. As a result, Fig. 11 presents the compared yield stress (Tabor relation, $\sigma_y \approx$ H/3 [49]) of NNT Cu from experimental data and the model predictions based on Eq. (6). According to Eq. (6), for example, the critical calculated λ is ~7.25 nm when the NG $d \approx 30$ nm, while it is ~16.8 nm for the NG with $d \approx 260$ nm. In our study, deformation NTs play a strengthening role when d is larger than 30 nm because the corresponding twin thickness is thicker than the critical λ. This result is consistent with previous reports that the NTs show an excellent mechanical stability in pure Cu when d is larger than ~30 nm [6]. However, NTs transform to a softening role when d is below 30 nm because the corresponding twin thickness is below the critical λ. It is indicated that the grain size and twin thickness effects on the strengthening mechanism reported in our study and previous prediction are universal in FCC twin-structured materials. For these small-size twin-free NGs, the softening behavior is dominated by pure GB-mediated plasticity.

5 Concluding remarks

In this work, GNS Cu layer containing both gradient NNT sub-layer region and extremely refined twin-free NG surface layer with grain size of ~ 10 nm has been achieved by the high-speed SPDT technique. Microstructure evolution and plastic deformation mechanisms of the NNT layer are atomically explored via HRTEM characterizations and MD simulations. First, the overall grain refinement process for GNS layer is gradually transited from dislocation activities-mediated mechanism in CGs and sub-grains to twinning-mediated mechanisms in UFGs with decreasing grain size in the deformed sub-surface region. Second, the deformation multifold twinning with zero-macrostrain is found to refine the microstructure for the formation of gradient NNT regions. Specifically, zero-macrostrain deformation multifold NTs can be formed by either immigration of 9R structural ITBs by cooperative activation of partials or RAP from GBs. However, the propensity of deformation NTs firstly increases and then decreases in small-size NGs once the grain size below ~ 48 nm and finally form extremely fine twin-free NGs at the topmost surface layer. The detwinning process of multifold NTs play a key role in the continual refinement of NGs as well. The detwinning process of multifold NTs is associated with the symmetry-breaking of the twin morphology (TBs migration, twin pole splitting and migration). Third, a GBs and TBs strengthening mechanism is found with the grain refinement from UFGs to NGs. However, a strengthening-softening transition is occurred when the grain size reduces to ~30 nm. The softening mechanism is attributed to the coupled effects of grain size and twin thickness on deformation method in NNT structures and the pure GB-mediated plasticity in extremely fine twin-free NGs. A series of critical twin thicknesses for softening in nanograins with different grain sizes are discussed to be consistent with our experimental statistics.

Acknowledgements

This work was supported by a grant from the Research Committee of PolyU under student account code RK25, National Natural Science Foundation of China Projects (Nos. 51701171 and 51971187), and the funding support to Partner State Key Laboratories in Hong Kong from the Innovation and Technology Commission (ITC) of the Government of the Hong Kong Special Administration Region (HKASR), China. The authors would also like to express their sincere thanks for the financial support from the PolyU Research Office (No. 1-BBXA). The assistance from SQ Yuan is also appreciated.

Competing interests

The authors declare no competing interests.

References

[1] E.O. Hall, The Deformation and Ageing of Mild Steel: II Characteristics of the Lüders Deformation, Proc. Phys. Soc. Sect. B. 64(9) (1951) pp. 747-753.

[2] N.J. Petch, The Cleavage Strength of Polycrystals, J. Iron. Steel. Inst. 174(1) (1953) pp. 25-28.

[3] K. Lu, Stabilizing nanostructures in metals using grain and twin boundary architectures, Nat. Rev. Mater. 1(5) (2016) pp. 16019.

[4] C.C. Koch, D.G. Morris, K. Lu, A. Inoue, Ductility of Nanostructured Materials, MRS Bull. 24(2) (2013) pp. 54-58.

[5] M.A. Meyers, A. Mishra, D.J. Benson, Mechanical properties of nanocrystalline materials, Prog. Mater. Sci. 51(4) (2006) pp. 427-556.

[6] X. Zhou, X. Li, K. Lu, Size Dependence of Grain Boundary Migration in Metals under Mechanical Loading, Phys. Rev. Lett. 122(12) (2019) pp. 126101.

[7] X. Zhou, X.Y. Li, K. Lu, Enhanced thermal stability of nanograined metals below a critical grain size, Science 360(6388) (2018) pp. 526-530.
[8] K. Lu, L. Lu, S. Suresh, Strengthening Materials by Engineering Coherent Internal Boundaries at the Nanoscale, Science 324(5925) (2009) pp. 349-352.
[9] L. Lu, R. Schwaiger, Z.W. Shan, M. Dao, K. Lu, S. Suresh, Nano-sized twins induce high rate sensitivity of flow stress in pure copper, Acta Mater. 53(7) (2005) pp. 2169-2179.
[10] X. Zhang, A. Misra, H. Wang, T.D. Shen, M. Nastasi, T.E. Mitchell, J.P. Hirth, R.G. Hoagland, J.D. Embury, Enhanced hardening in Cu/330 stainless steel multilayers by nanoscale twinning, Acta Mater. 52(4) (2004) pp. 995-1002.
[11] L. Lu, Y. Shen, X. Chen, L. Qian, K. Lu, Ultrahigh Strength and High Electrical Conductivity in Copper, Science 304(5669) (2004) pp. 422-426.
[12] Y. Tian, B. Xu, D. Yu, Y. Ma, Y. Wang, Y. Jiang, W. Hu, C. Tang, Y. Gao, K. Luo, Z. Zhao, L.-M. Wang, B. Wen, J. He, Z. Liu, Ultrahard nanotwinned cubic boron nitride, Nature 493 (2013) pp. 385.
[13] Q. Huang, D. Yu, B. Xu, W. Hu, Y. Ma, Y. Wang, Z. Zhao, B. Wen, J. He, Z. Liu, Y. Tian, Nanotwinned diamond with unprecedented hardness and stability, Nature 510(7504) (2014) pp. 250-253.
[14] X. Zhou, Z. Feng, L. Zhu, J. Xu, L. Miyagi, H. Dong, H. Sheng, Y. Wang, Q. Li, Y. Ma, H. Zhang, J. Yan, N. Tamura, M. Kunz, K. Lutker, T. Huang, D.A. Hughes, X. Huang, B. Chen, High-pressure strengthening in ultrafine-grained metals, Nature 579(7797) (2020) pp. 67-72.
[15] X. Ke, J. Ye, Z. Pan, J. Geng, M.F. Besser, D. Qu, A. Caro, J. Marian, R.T. Ott, Y.M. Wang, F. Sansoz, Ideal maximum strengths and defect-induced softening in nanocrystalline-nanotwinned metals, Nature Mater. 18(11) (2019) pp. 1207-1214.
[16] L. Lu, X. Chen, X. Huang, K. Lu, Revealing the maximum strength in nanotwinned copper, Science 323(5914) (2009) pp. 607-610.
[17] N. Lu, K. Du, L. Lu, H.Q. Ye, Transition of dislocation nucleation induced by local stress concentration in nanotwinned copper, Nature Commun. 6 (2015) pp. 7648.
[18] L. Wang, K. Du, C. Yang, J. Teng, L. Fu, Y. Guo, Z. Zhang, X. Han, In situ atomic-scale observation of grain size and twin thickness effect limit in twin-structural nanocrystalline platinum, Nature Commun. 11(1) (2020) pp. 1167.
[19] X. Li, Y. Wei, L. Lu, K. Lu, H. Gao, Dislocation nucleation governed softening and maximum strength in nano-twinned metals, Nature 464(7290) (2010) pp. 877-80.
[20] L. Zhu, H. Ruan, X. Li, D. Ming, L. Jian, Modeling grain size dependent optimal twin spacing for achieving ultimate high strength and related high ductility in nanotwinned metals, Acta Mater. 59(14) (2011) pp. 5544-5557.
[21] Wei, Yujie, Scaling of maximum strength with grain size in nanotwinned fcc metals, Phys. Rev. B 83(13) (2011) pp. 132104.
[22] E. Ma, T. Zhu, Towards strength–ductility synergy through the design of heterogeneous nanostructures in metals, Mater. Today 20(6) (2017) pp. 323-331.
[23] T.H. Fang, W.L. Li, N.R. Tao, K. Lu, Revealing Extraordinary Intrinsic Tensile Plasticity in Gradient Nano-Grained Copper, Science 331(6024) (2011) pp. 1587-1590.
[24] K. Lu, Making strong nanomaterials ductile with gradients, Science 345(6203) (2014) pp. 1455-1456.
[25] A. Chen, J. Liu, H. Wang, J. Lu, Y.M. Wang, Gradient twinned 304 stainless steels for high strength and high ductility, Mater. Sci. Eng. A 667 (2016) pp. 179-188.
[26] X.Y. Li, Z.H. Jin, X. Zhou, K. Lu, Constrained minimal-interface structures in polycrystalline copper with extremely fine grains, Science 370(6518) (2020) pp. 831-836.

[27] X.C. Liu, H.W. Zhang, K. Lu, Strain-induced ultrahard and ultrastable nanolaminated structure in nickel, Science 342(6156) (2013) pp. 337-340.
[28] X.Z. Liao, Y.H. Zhao, S.G. Srinivasan, Y.T. Zhu, R.Z. Valiev, D.V. Gunderov, Deformation twinning in nanocrystalline copper at room temperature and low strain rate, App. Phys. Lett. 84(4) (2004) pp. 592-594.
[29] S. Suet To, V.H. Wang, W.B. Lee, Single Point Diamond Turning Technology, Materials Characterisation and Mechanism of Micro-Cutting in Ultra-Precision Diamond Turning, Springer Berlin Heidelberg, Berlin, Heidelberg, 2018, pp. 3-6.
[30] H. Fu, X. Zhou, B. Wu, L. Qian, X.-S. Yang, Atomic-scale dissecting the formation mechanism of gradient nanostructured layer on Mg alloy processed by a novel high-speed machining technique, J. Mater. Sci. Technol. 82 (2021) pp. 227-238.
[31] Y. Mishin, M. Mehl, D. Papaconstantopoulos, A. Voter, J. Kress, Structural stability and lattice defects in copper: Ab initio, tight-binding, and embedded-atom calculations, Phys. Rev. B 63(22) (2001) pp. 224106.
[32] Y.S. Li, N.R. Tao, K. Lu, Microstructural evolution and nanostructure formation in copper during dynamic plastic deformation at cryogenic temperatures, Acta Mater. 56(2) (2008) pp. 230-241.
[33] Y.T. Zhu, X.Z. Liao, R.Z. Valiev, Formation mechanism of fivefold deformation twins in nanocrystalline face-centered-cubic metals, Appl. Phys. Lett. 86(10) (2005) pp. 103112.
[34] X.H. An, Q.Y. Lin, S.D. Wu, Z.F. Zhang, R.B. Figueiredo, N. Gao, T.G. Langdon, Formation of fivefold deformation twins in an ultrafine-grained copper alloy processed by high-pressure torsion, Scripta Mater. 64(3) (2011) pp. 249-252.
[35] X. Liu, L. Sun, L. Zhu, J. Liu, K. Lu, J. Lu, High-order hierarchical nanotwins with superior strength and ductility, Acta Mater. 149 (2018) pp. 397-406.
[36] A.Y. Chen, L.L. Zhu, L.G. Sun, J.B. Liu, H.T. Wang, X.Y. Wang, J.H. Yang, J. Lu, Scale law of complex deformation transitions of nanotwins in stainless steel, Nature Commun. 10(1) (2019) pp. 1403.
[37] M. Song, Z. Wu, N. Lu, D. Li, Strain Relaxation-Induced Twin Interface Migration and Morphology Evolution of Silver Nanoparticles, Chem. Mater. 31(3) (2019) pp. 842-850.
[38] M. Song, G. Zhou, N. Lu, J. Lee, E. Nakouzi, H. Wang, D. Li, Oriented attachment induces fivefold twins by forming and decomposing high-energy grain boundaries, Science 367(6473) (2020) pp. 40-45.
[39] L. Liu, J. Wang, S.K. Gong, S.X. Mao, High resolution transmission electron microscope observation of zero-strain deformation twinning mechanisms in Ag, Phys. Rev. Lett. 106(17) (2011) pp. 175504.
[40] X.L. Wu, X.Z. Liao, S.G. Srinivasan, F. Zhou, E.J. Lavernia, R.Z. Valiev, Y.T. Zhu, New Deformation Twinning Mechanism Generates Zero Macroscopic Strain in Nanocrystalline Metals, Phys. Rev. Lett. 100(9) (2008) pp. 095701.
[41] J.Y. Zhang, P. Zhang, R.H. Wang, G. Liu, G.J. Zhang, J. Sun, Grain-size-dependent zero-strain mechanism for twinning in copper, Phys. Rev. B 86(6) (2012) pp.
[42] Z.H. Cao, L.J. Xu, W. Sun, J. Shi, M.Z. Wei, G.J. Pan, X.B. Yang, J.W. Zhao, X.K. Meng, Size dependence and associated formation mechanism of multiple-fold annealing twins in nanocrystalline Cu, Acta Mater. 95 (2015) pp. 312-323.
[43] A. Chokshi, A. Rosen, J. Karch, H. Gleiter, On the validity of the Hall-Petch relationship in nanocrystalline materials, Scripta Metall. 23(10) (1989) pp. 1679-1684.
[44] G.E. Fougere, J.R. Weertman, R.W. Siegel, S. Kim, Grain-size dependent hardening and softening of nanocrystalline Cu and Pd, Scripta Metall. 26(12) (1992) pp. 1879-1883.
[45] R. Suryanarayanan Iyer, C.A. Frey, S.M.L. Sastry, B.E. Waller, W.E. Buhro, Plastic deformation of

nanocrystalline Cu and Cu–0.2 wt.% B, Mater. Sci. Eng. A 264(1) (1999) pp. 210-214.
[46] P.G. Sanders, J.A. Eastman, J.R. Weertman, Elastic and tensile behavior of nanocrystalline copper and palladium, Acta Mater. 45(10) (1997) pp. 4019-4025.
[47] Y.S. Zhang, Z. Han, K. Wang, K. Lu, Friction and wear behaviors of nanocrystalline surface layer of pure copper, Wear 260(9-10) (2006) pp. 942-948.
[48] M.R. Akbarpour, H.S. Kim, Microstructure, grain growth, and hardness during annealing of nanocrystalline Cu powders synthesized via high energy mechanical milling, Mater. Des. 83 (2015) pp. 644-650.
[49] D. Tabor, The hardness of metals, Oxford university press, 2000.
[50] M. Haouaoui, I. Karaman, K. Harwig, H. Maier, Microstructure evolution and mechanical behavior of bulk copper obtained by consolidation of micro-and nanopowders using equal-channel angular extrusion, Metall. Mater. Trans. A 35(9) (2004) pp. 2935-2949.
[51] K.X. Wei, J. Horky, W. Wei, M.J. Zehetbauer, D. Setman, E. Schafler, J. Hu, Enhancing tensile properties of Cu and Cu-Al alloys cryogenically processed by high pressure torsion, J. Alloys Comp. 771 (2019) pp. 317-321.
[52] H. Jiang, Y.T. Zhu, D.P. Butt, I.V. Alexandrov, T.C. Lowe, Microstructural evolution, microhardness and thermal stability of HPT-processed Cu, Mater. Sci. Eng. A 290(1) (2000) pp. 128-138.
[53] Y.H. Zhao, J.F. Bingert, X.Z. Liao, B.Z. Cui, K. Han, A.V. Sergueeva, A.K. Mukherjee, R.Z. Valiev, T.G. Langdon, Y.T. Zhu, Simultaneously Increasing the Ductility and Strength of Ultra-Fine-Grained Pure Copper, Adv. Mater. 18(22) (2006) pp. 2949-2953.
[54] N. Lugo, N. Llorca, J.J. Suñol, J.M. Cabrera, Thermal stability of ultrafine grains size of pure copper obtained by equal-channel angular pressing, J. Mater. Sci. 45(9) (2010) pp. 2264-2273.
[55] A. Fattah-alhosseini, O. Imantalab, Y. Mazaheri, M.K. Keshavarz, Microstructural evolution, mechanical properties, and strain hardening behavior of ultrafine grained commercial pure copper during the accumulative roll bonding process, Mater. Sci. Eng. A 650 (2016) pp. 8-14.
[56] Y.T. Zhu, J. Narayan, J.P. Hirth, S. Mahajan, X.L. Wu, X.Z. Liao, Formation of single and multiple deformation twins in nanocrystalline fcc metals, Acta Mater. 57(13) (2009) pp. 3763-3770.
[57] V. Yamakov, D. Wolf, S.R. Phillpot, A.K. Mukherjee, H. Gleiter, Dislocation processes in the deformation of nanocrystalline aluminium by molecular-dynamics simulation, Nature Mater. 1(1) (2002) pp. 45-8.
[58] Y.T. Zhu, X.Z. Liao, X.L. Wu, Deformation twinning in bulk nanocrystalline metals: Experimental observations, JOM 60(9) (2008) pp. 60-64.
[59] M. Chen, E. Ma, K.J. Hemker, H. Sheng, Y. Wang, X. Cheng, Deformation twinning in nanocrystalline aluminum, Sci. Adv. 300 (2003) pp. 1275-1278.
[60] P.M. Anderson, J.P. Hirth, J. Lothe, Theory of dislocations, Cambridge University Press, 2017.
[61] Y.T. Zhu, X.Z. Liao, X.L. Wu, J. Narayan, Grain size effect on deformation twinning and detwinning, J. Mater. Sci. 48(13) (2013) pp. 4467-4475.
[62] C.X. Huang, K. Wang, S.D. Wu, Z.F. Zhang, G.Y. Li, S.X. Li, Deformation twinning in polycrystalline copper at room temperature and low strain rate, Acta Mater. 54(3) (2006) pp. 655-665.
[63] Y.T. Zhu, X.L. Wu, X.Z. Liao, J. Narayan, L.J. Kecskés, S.N. Mathaudhu, Dislocation–twin interactions in nanocrystalline fcc metals, Acta Mater.59(2) (2011) pp. 812-821.
[64] L. Sun, X. He, J. Lu, Nanotwinned and hierarchical nanotwinned metals: a review of experimental, computational and theoretical efforts, NPJ Comput. Mater. 4(1) (2018) pp. 1-18.